The phase diagram of three-flavor quark matter under compact star constraints

D. Blaschke,[1,*] S. Fredriksson,[2,†] H. Grigorian,[3,‡] A.M. Öztaş,[4,§] and F. Sandin[2,¶]

[1] *Gesellschaft für Schwerionenforschung mbH (GSI), D-64291 Darmstadt, Germany, and Bogoliubov Laboratory for Theoretical Physics, JINR Dubna, 141980 Dubna, Russia*
[2] *Department of Physics, Luleå University of Technology, SE-97187 Luleå, Sweden*
[3] *Institut für Physik, Universität Rostock, D-18051 Rostock, Germany, and Department of Physics, Yerevan State University,375025 Yerevan, Armenia*
[4] *Department of Physics, Hacettepe University, TR-06532 Ankara, Turkey*

The phase diagram of three-flavor quark matter under compact star constraints is investigated within a Nambu–Jona-Lasinio model. Local color and electric charge neutrality is imposed for β-equilibrated superconducting quark matter. The constituent quark masses and the diquark condensates are determined selfconsistently in the plane of temperature and quark chemical potential. Both strong and intermediate diquark coupling strengths are considered. We show that in both cases, gapless superconducting phases do not occur at temperatures relevant for compact star evolution, i.e., below $T \sim 50$ MeV. The stability and structure of isothermal quark star configurations are evaluated. For intermediate coupling, quark stars are composed of a mixed phase of normal (NQ) and two-flavor superconducting (2SC) quark matter up to a maximum mass of 1.21 $M_\odot$. At higher central densities, a phase transition to the three-flavor color flavor locked (CFL) phase occurs and the configurations become unstable. For the strong diquark coupling we find stable stars in the 2SC phase, with masses up to 1.326 $M_\odot$. A second family of more compact configurations (twins) with a CFL quark matter core and a 2SC shell is also found to be stable. The twins have masses in the range 1.301...1.326 $M_\odot$. We consider also hot isothermal configurations at temperature $T = 40$ MeV. When the hot maximum mass configuration cools down, due to emission of photons and neutrinos, a mass defect of 0.1 $M_\odot$ occurs and two final state configurations are possible.

PACS numbers: 12.38.Mh, 24.85.+p, 26.60.+c, 97.60.-s

I. INTRODUCTION

Theoretical investigations of the QCD phase diagram at high densities have recently gained momentum due to results of non-perturbative low-energy QCD models [1, 2, 3] of color superconductivity in quark matter [4, 5]. These models predict that the diquark pairing condensates are of the order of 100 MeV and a remarkably rich phase structure has been identified [6, 7, 8, 9]. The main motivation for studying the low-temperature domain of the QCD phase diagram is its possible relevance for the physics of compact stars [10, 11, 12]. Observable effects of color superconducting phases in compact stars is expected, e.g., in the cooling behaviour [13, 14, 15, 16, 17], magnetic field evolution [18, 19, 20, 21], and in burst-type phenomena [22, 23, 24, 25].

The most prominent color superconducting phases with large diquark pairing gaps are the two-flavor scalar diquark condensate (2SC) and the color-flavor locking (CFL) condensate. The latter requires approximate SU(3) flavor symmetry and occurs therefore only at rather large quark chemical potentials, $\mu_q > 430 - 500$ MeV, of the order of the dynamically generated strange quark mass M_s, whereas the 2SC phase can appear already at the chiral restoration transition for $\mu_q > 330 - 350$ MeV [26, 27, 28]. Note that the quark chemical potential in the center of a typical compact star is expected to not exceed a value of ~ 500 MeV so the volume fraction of a strange quark matter phase will be insufficient to entail observable consequences. However, when the strange quark mass is considered not dynamically, but as a free parameter independent of the thermodynamical conditions, it has been shown that for not too large M_s the CFL phase dominates over the 2SC phase [29, 30]. Studies of the QCD phase diagram with fixed strange quark mass have recently been extended to the discussion of gapless CFL (gCFL) phases [31, 32, 33]. The gapless phases occur when the asymmetry between Fermi levels of different flavors is large enough to allow for zero energy excitations while a finite pairing gap exists. They have been found first for the 2SC phase (g2SC) within a dynamical chiral quark model [34, 35].

Any scenario for compact star evolution that is based on the occurence of quark matter relies on the assumptions about the properties of this phase. It is therefore of prior importance to obtain a phase diagram of three-flavor quark matter under compact star constraints with selfconsistently determined dynamical quark masses. In the present paper we will employ the Nambu–Jona-Lasinio (NJL) model to delineate the different quark matter phases in the plane of temperature and chemical potential. We also address the question whether CFL quark matter and gapless phases are likely to play a role in compact star interiors.

*Electronic address: Blaschke@theory.gsi.de
†Electronic address: Sverker.Fredriksson@ltu.se
‡Electronic address: Hovik.Grigorian@uni-rostock.de
§Electronic address: oztas@hacettepe.edu.tr
¶Electronic address: Fredrik.Sandin@ltu.se

II. MODEL

In this paper, we consider an NJL model with quark-antiquark interactions in the color singlet scalar/pseudoscalar channel, and quark-quark interactions in the scalar color antitriplet channel. We neglect the less attractive interaction channels, e.g., the isospin-singlet channel, which could allow for weak spin-1 condensates. Such condensates allow for gapless excitations at low temperatures and could be important for the cooling behaviour of compact stars. However, the coupling strengths in these channels are poorly known and we therefore neglect them here. The Lagrangian density is is given by

$$\begin{aligned}\mathcal{L} &= \bar{q}_{i\alpha}(i\partial\!\!\!/\delta_{ij}\delta_{\alpha\beta} - M^0_{ij}\delta_{\alpha\beta} + \mu_{ij,\alpha\beta}\gamma^0)q_{j\beta} \\ &+ G_S\sum_{a=0}^{8}\left[(\bar{q}\tau^a_f q)^2 + (\bar{q}i\gamma_5\tau^a_f q)^2\right] \\ &+ G_D\sum_{k,\gamma}\left[(\bar{q}_{i\alpha}\epsilon_{ijk}\epsilon_{\alpha\beta\gamma}q^C_{j\beta})(\bar{q}^C_{i'\alpha'}\epsilon_{i'j'k}\epsilon_{\alpha'\beta'\gamma}q_{j'\beta'})\right. \\ &+ \left.(\bar{q}_{i\alpha}i\gamma_5\epsilon_{ijk}\epsilon_{\alpha\beta\gamma}q^C_{j\beta})(\bar{q}^C_{i'\alpha'}i\gamma_5\epsilon_{i'j'k}\epsilon_{\alpha'\beta'\gamma}q_{j'\beta'})\right], \quad (1)\end{aligned}$$

where $M^0_{ij} = \mathrm{diag}(m^0_u, m^0_d, m^0_s)$ is the current quark mass matrix in flavor space and $\mu_{ij,\alpha\beta}$ is the chemical potential matrix in color and flavor space. Due to strong and weak interactions, the various chemical potentials are not independent. In the superconducting phases a $U(1)$ gauge symmetry remains unbroken [36], and the associated charge is a linear combination of the electric charge, Q, and two orthogonal generators of the unbroken $SU(2)_c$ symmetry. Hence, there are in total four independent chemical potentials

$$\mu_{ij,\alpha\beta} = (\mu\delta_{ij} + Q\mu_Q)\delta_{\alpha\beta} + (T_3\mu_3 + T_8\mu_8)\delta_{ij}, \quad (2)$$

where $Q = \mathrm{diag}(2/3, -1/3, -1/3)$ is the electric charge in flavor space, and $T_3 = \mathrm{diag}(1, -1, 0)$ and $T_8 = \mathrm{diag}(1/\sqrt{3}, 1/\sqrt{3}, -2/\sqrt{3})$ are the generators in color space. The quark number chemical potential, μ, is related to the baryon chemical potential by $\mu = \mu_B/3$. The quark fields in color, flavor and Dirac spaces are denoted by $q_{i\alpha}$ and $\bar{q}_{i\alpha} = q^\dagger_{i\alpha}\gamma^0$. τ^a_f are Gell-Mann matrices acting in flavor space. Charge conjugated quark fields are denoted by $q^C = C\bar{q}^T$ and $\bar{q}^C = q^T C$, where $C = i\gamma^2\gamma^0$ is the Dirac charge conjugation matrix. The indices α, β and γ represent colors ($r = 1$, $g = 2$ and $b = 3$), while i, j and k represent flavors ($u = 1$, $d = 2$ and $s = 3$). G_S and G_D are dimensionful coupling constants that must be determined by experiments.

Typically, three-flavor NJL models use a 't Hooft determinant interaction that induces a $\mathrm{U}_A(1)$ symmetry breaking in the pseudoscalar isoscalar meson sector which can be adjusted such that the η-η' mass difference is described. This realization of the $\mathrm{U}_A(1)$ breaking leads to the important consequence that the quark condensates of different flavor sectors get coupled. The dynamically generated strange quark mass contains a contribution from the chiral condensates of the light flavors. There is, however, another possible realization of the $\mathrm{U}_A(1)$ symmetry breaking that does not arise on the mean field level, but only for the mesonic fluctuations in the pseudoscalar isoscalar channel. This is due to the coupling to the non-perturbative gluon sector via the the triangle anomaly, see e.g. [37, 38, 39]. This realization of the η-η' mass difference gives no contribution to the quark thermodynamics at the mean field level, which we will follow in this paper. Up to now it is not known, which of the two $\mathrm{U}_A(1)$ breaking mechanisms is the dominant one in nature. In the present exploratory study of the mean field thermodynamics of three-flavor quark matter, we will take the point of view that the 't Hooft term might be subdominant and can be disregarded. One possible way to disentangle both mechanisms is due to their different response to chiral symmetry restoration at finite temperatures and densities. While in heavy-ion collisions only the finite temperature aspect can be systematically studied [40], the state of matter in neutron star interiors may be suitable to probe the $\mathrm{U}_A(1)$ symmetry restoration and its possible implications for the quark matter phase diagram at high densities and low temperatures. A comparison of the results presented in this work with the alternative treatment of the phase diagram of three-flavor quark matter including the 't Hooft determinant term, see [41], may therefore be very instructive.

The mean-field Lagrangian is

$$\begin{aligned}\mathcal{L}^{MF} &= \bar{q}_{i\alpha}\left[i\partial\!\!\!/\delta_{ij}\delta_{\alpha\beta} - (M^0_{ij} - 4G_S\langle\!\langle\bar{q}_{i\alpha}q_{j\beta}\rangle\!\rangle\delta_{ij})\delta_{\alpha\beta} + \mu_{ij,\alpha\beta}\gamma^0\right]q_{j\beta} \\ &- 2G_S\sum_i\langle\!\langle\bar{q}_i q_i\rangle\!\rangle^2 - \sum_{k,\gamma}\frac{|\Delta_{k\gamma}|^2}{4G_D} + \bar{q}_{i\alpha}\frac{\widetilde{\Delta}_{k\gamma}}{2}q^C_{j\beta} + \bar{q}^C_{i\alpha}\frac{\widetilde{\Delta}^\dagger_{k\gamma}}{2}q_{j\beta}, \quad (3)\\ \widetilde{\Delta}_{k\gamma} &= 2G_D i\gamma_5\epsilon_{\alpha\beta\gamma}\epsilon_{ijk}\langle\!\langle\bar{q}_{i'\alpha'}i\gamma_5\epsilon_{\alpha'\beta'\gamma}\epsilon_{i'j'k}q^C_{j'\beta'}\rangle\!\rangle = i\gamma_5\epsilon_{\alpha\beta\gamma}\epsilon_{ijk}\Delta_{k\gamma}. \quad (4)\end{aligned}$$

We define the chiral gaps

$$\phi_i = -4G_S\langle\!\langle\bar{q}_i q_i\rangle\!\rangle, \quad (5)$$

and the diquark gaps

$$\Delta_{k\gamma} = 2G_D\langle\!\langle\bar{q}_{i\alpha}i\gamma_5\epsilon_{\alpha\beta\gamma}\epsilon_{ijk}q^C_{j\beta}\rangle\!\rangle. \quad (6)$$

The chiral condensates contribute to the dynamical mass of the quarks, the constituent quark mass matrix in flavor space is $M = \mathrm{diag}(m_u^0 + \phi_u, m_d^0 + \phi_d, m_s^0 + \phi_s)$, where m_i^0 are the current quark masses. For finite current quark masses the $U(3)_L \times U(3)_R$ symmetry of the Lagrangian is spontaneously broken and only approximately restored at high densities.

The diquark gaps, $\Delta_{k\gamma}$, are antisymmetric in flavor and color, e.g., the condensate corresponding to Δ_{ur} is created by green and blue down and strange quarks. Due to this property, the diquark gaps can be denoted with the flavor indices of the interacting quarks

$$\Delta_{ur} = \Delta_{ds}, \quad \Delta_{dg} = \Delta_{us}, \quad \Delta_{sb} = \Delta_{ud}. \tag{7}$$

After reformulating the mean-field lagrangian in 8-component Nambu-Gorkov spinors [42, 43] and performing the functional integrals over Grassman variables [44] we obtain the thermodynamic potential

$$\begin{aligned}\Omega(T,\mu) &= \frac{\phi_u^2+\phi_d^2+\phi_s^2}{8G_S} + \frac{|\Delta_{ud}|^2+|\Delta_{us}|^2+|\Delta_{ds}|^2}{4G_D} \\ &- T\sum_n \int \frac{d^3p}{(2\pi)^3}\frac{1}{2}\mathrm{Tr}\ln\left(\frac{1}{T}S^{-1}(i\omega_n,\vec{p})\right) \\ &+ \Omega_e - \Omega_0. \end{aligned} \tag{8}$$

Here $S^{-1}(p)$ is the inverse propagator of the quark fields at four momentum $p = (i\omega_n, \vec{p})$,

$$S^{-1}(i\omega_n,\vec{p}) = \begin{bmatrix} \not{p} - M + \mu\gamma^0 & \widetilde{\Delta}_{k\gamma} \\ \widetilde{\Delta}^\dagger_{k\gamma} & \not{p} - M - \mu\gamma^0 \end{bmatrix}, \tag{9}$$

and $\omega_n = (2n+1)\pi T$ are the Matsubara frequencies for fermions. The thermodynamic potential of ultrarelativistic electrons,

$$\Omega_e = -\frac{1}{12\pi^2}\mu_Q^4 - \frac{1}{6}\mu_Q^2 T^2 - \frac{7}{180}\pi^2 T^4, \tag{10}$$

has been added to the potential, and the vacuum contribution,

$$\begin{aligned}\Omega_0 = \Omega(0,0) &= \frac{\phi_{0u}^2+\phi_{0d}^2+\phi_{0s}^2}{8G_S} \\ &-2N_c\sum_i \int \frac{d^3p}{(2\pi)^3}\sqrt{M_i^2+p^2}, \end{aligned} \tag{11}$$

has been subtracted in order to get zero pressure in vacuum. Using the identity $\mathrm{Tr}(\ln(D)) = \ln(\det(D))$ and evaluating the determinant (see Appendix A), we obtain

$$\ln\det\left(\frac{1}{T}S^{-1}(i\omega_n,\vec{p})\right) = 2\sum_{a=1}^{18}\ln\left(\frac{\omega_n^2+\lambda_a(\vec{p})^2}{T^2}\right). \tag{12}$$

The quasiparticle dispersion relations, $\lambda_a(\vec{p})$, are the eigenvalues of the Hermitian matrix,

$$\mathcal{M} = \begin{bmatrix} -\gamma^0\vec{\gamma}\cdot\vec{p} - \gamma^0 M + \mu & \gamma^0\widetilde{\Delta}_{k\gamma}C \\ \gamma^0 C\widetilde{\Delta}^\dagger_{k\gamma} & -\gamma^0\vec{\gamma}^T\cdot\vec{p} + \gamma^0 M - \mu \end{bmatrix}, \tag{13}$$

in color, flavor, and Nambu-Gorkov space. This result is in agreement with [30, 41]. Finally, the Matsubara sum can be evaluated on closed form [44],

$$T\sum_n \ln\left(\frac{\omega_n^2+\lambda_a^2}{T^2}\right) = \lambda_a + 2T\ln(1+e^{-\lambda_a/T}), \tag{14}$$

leading to an expression for the thermodynamic potential on the form

$$\begin{aligned}\Omega(T,\mu) &= \frac{\phi_u^2+\phi_d^2+\phi_s^2}{8G_S} + \frac{|\Delta_{ud}|^2+|\Delta_{us}|^2+|\Delta_{ds}|^2}{4G_D} \\ &- \int\frac{d^3p}{(2\pi)^3}\sum_{a=1}^{18}\left(\lambda_a + 2T\ln\left(1+e^{-\lambda_a/T}\right)\right) \\ &+ \Omega_e - \Omega_0. \end{aligned} \tag{15}$$

It should be noted that (14) is an even function of λ_a, so the signs of the quasiparticle dispersion relations are arbitrary. In this paper, we assume that there are no trapped neutrinos. This approximation is valid for quark matter in neutron stars, after the short period of deleptonization is over.

Equations (10), (11), (13), and (15) form a consistent thermodynamic model of superconducting quark matter. The independent variables are μ and T. The gaps, ϕ_i, and Δ_{ij}, are variational order parameters that should be determined by minimization of the grand canonical thermodynamical potential, Ω. Also, quark matter should be locally color and electric charge neutral, so at the physical minima of the thermodynamic potential the corresponding number densities should be zero

$$n_Q = -\frac{\partial\Omega}{\partial\mu_Q} = 0, \tag{16}$$

$$n_8 = -\frac{\partial\Omega}{\partial\mu_3} = 0, \tag{17}$$

$$n_3 = -\frac{\partial\Omega}{\partial\mu_8} = 0. \tag{18}$$

The pressure, P, is related to the thermodynamic potential by $P = -\Omega$ at the global minima of Ω. The quark density, entropy and energy density are then obtained as derivatives of the thermodynamical potential with respect to μ, T and $1/T$, respectively.

III. RESULTS

The numerical solutions to be reported in this Section are obtained with the following set of model parameters, taken from Table 5.2 of Ref. [8] for vanishing 't Hooft interaction,

$$m_{u,d}^0 = 5.5\ MeV\ , \tag{19}$$

$$m_s^0 = 112.0\ MeV\ , \tag{20}$$

$$G_S\Lambda^2 = 2.319\ , \tag{21}$$

$$\Lambda^2 = 602.3\ MeV\ . \tag{22}$$

With these parameters, the following low-energy QCD observables can be reproduced: $m_\pi = 135$ MeV, $m_K = 497.7$ MeV, $f_\pi = 92.4$ MeV. The value of the diquark coupling strength $G_D = \eta G_S$ is considered as a free parameter of the model. Here we present results for $\eta = 0.75$ (intermediate coupling) and $\eta = 1.0$ (strong coupling).

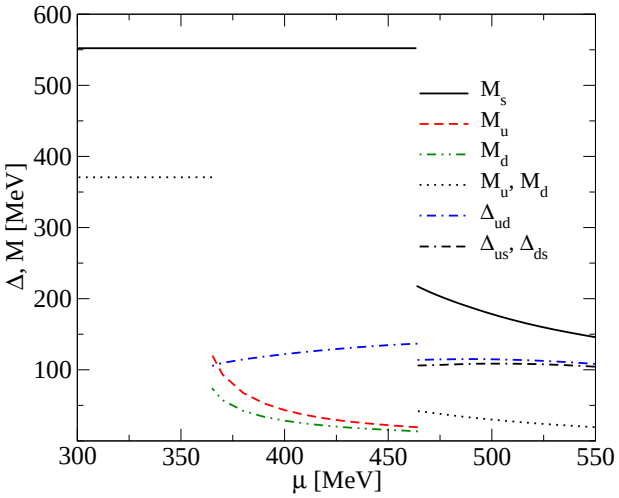

FIG. 1: Gaps and dynamical quark masses as a function of μ at T=0 for intermediate diquark coupling, $\eta = 0.75$.

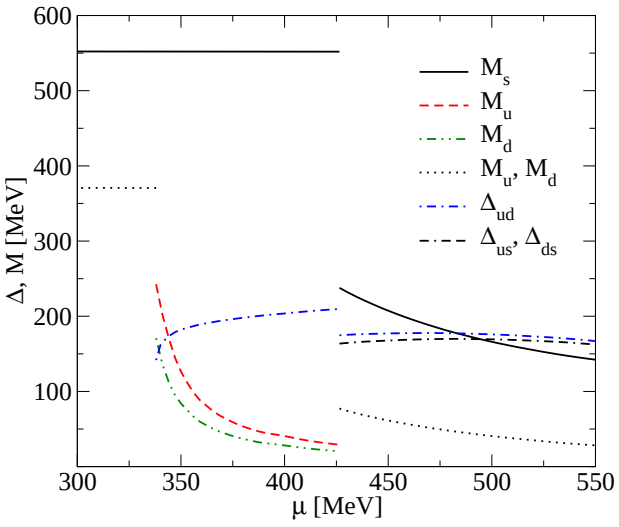

FIG. 2: Gaps and dynamical quark masses as a function of μ at T=0 for strong diquark coupling, $\eta = 1$.

A. Quark masses and pairing gaps at zero temperature

The dynamically generated quark masses and the diquark pairing gaps are determined selfconsistently at the absolute minima of the thermodynamic potential, in the plane of temperature and quark chemical potential. This is done for both the strong and the intermediate diquark coupling strength. In Figs. 1 and 2 we show the dependence of masses and gaps on the quark chemical potential at $T = 0$ for $\eta = 0.75$ and $\eta = 1.0$, resp. A

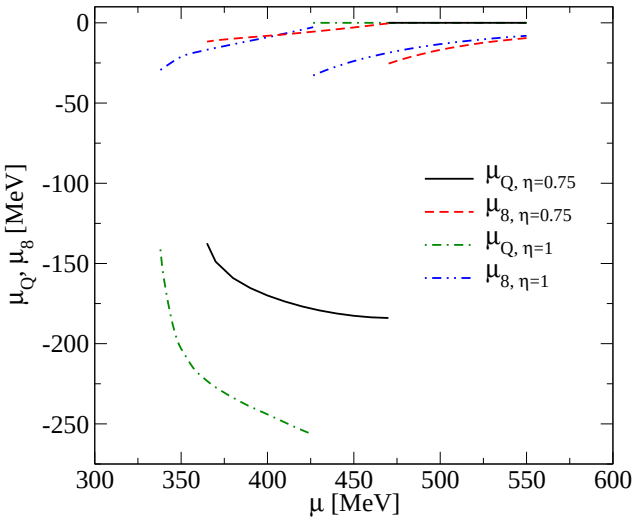

FIG. 3: Chemical potentials μ_Q and μ_8 at T=0 for both values of the diquark coupling $\eta = 0.75$ and $\eta = 1$. All phases considered in this work have zero n_3 color charge for $\mu_3 = 0$, hence μ_3 is omitted in the plot.

characteristic feature of this dynamical quark model is that the critical quark chemical potentials where light and strange quark masses jump from their constituent mass values down to almost their current mass values do not coincide. With increasing chemical potential the system undergoes a sequence of two transitions: (1) vacuum → two-flavor quark matter, (2) two-flavor → three-flavor quark matter. The intermediate two-flavor quark matter phase occurs within an interval of chemical potentials typical for compact star interiors. While at intermediate coupling the asymmetry between of up and down quark chemical potentials leads to a mixed NQ-2SC phase below temperatures of 20-30 MeV, at strong coupling the pure 2SC phase extends down to T=0. Simultaneously, the limiting chemical potentials of the two-flavor quark matter region are lowered by about 40 MeV. Three-flavor quark matter is always in the CFL phase where all quarks are paired. The robustness of the 2SC condensate under compact star constraints, with respect to changes of the coupling strength, as well as to a softening of the momentum cutoff by a formfactor, has been recently investigated within a different parametrization [45] with

similar trend: for $\eta = 0.75$ and NJL formfactor the 2SC condensate does not occur for moderate chemical potentials while for $\eta = 1.0$ it occurs simultaneously with chiral symmetry restoration. Fig. 3 shows the corresponding dependences of the chemical potentials conjugate to electric (μ_Q) and color (μ_8) charges. All phases considered in this work have zero n_3 color charge for $\mu_3 = 0$.

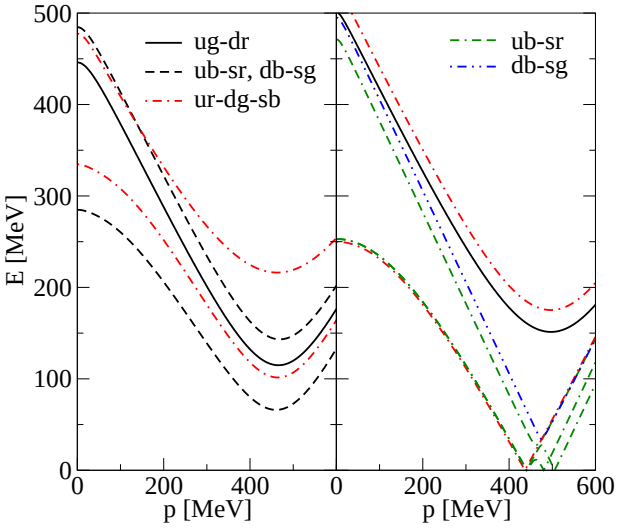

FIG. 4: Quark-quark quasiparticle dispersion relations. For $\eta = 0.75$, $T = 0$, and $\mu = 480$ MeV (left panel) there is a forbidden energy band above the Fermi surface. All dispersion relations are gapped at this point in the $\mu - T$ plane, see Fig. 5. There is no forbidden energy band for the $ub - sr$, $db - sq$, and $ur - dg - sb$ quasiparticles at $\eta = 1$, $T = 84$ MeV, and $\mu = 500$ MeV (right panel). This point in the $\mu - T$ plane constitute a part of the gapless CFL phase of Fig. 6.

B. Dispersion relations and gapless phases

In Fig. 4 we show the quasiparticle dispersion relations of different excitations at two points in the phase diagram: (I) the CFL phase (left panel), where there is a finite energy gap for all dispersion relations. (II) the gCFL phase (right panel), where the energy spectrum is shifted due to the assymetry in the chemical potentials, such that the CFL gap is zero and (gapless) excitations with zero energy are possible. In the present model, this phenomenon occurs only at rather high temperatures, where the condensates are diminished by thermal fluctuations.

C. Phase diagram

The thermodynamical state of the system is characterized by the values of the order parameters and their dependence on T and μ. Here we illustrate this dependency

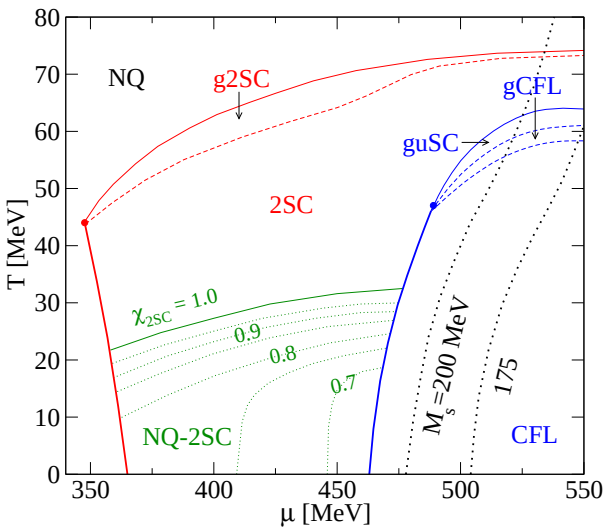

FIG. 5: Phase diagram of neutral three-flavor quark matter for intermediate diquark coupling $\eta = 0.75$. First-order phase transition boundaries are indicated by bold solid lines, while thin solid lines correspond to second-order phase boundaries. The dashed lines indicate gapless phase boundaries. The volume fraction, χ_{2SC}, of the 2SC component of the mixed NQ-2SC phase is denoted with thin dotted lines, while the constituent strange quark mass is denoted with bold dotted lines.

in a phase diagram. We identify the following phases:

1. NQ: $\Delta_{ud} = \Delta_{us} = \Delta_{ds} = 0$;
2. NQ-2SC: $\Delta_{ud} \neq 0$, $\Delta_{us} = \Delta_{ds} = 0$, $0 < \chi_{2SC} < 1$;
3. 2SC: $\Delta_{ud} \neq 0$, $\Delta_{us} = \Delta_{ds} = 0$;
4. uSC: $\Delta_{ud} \neq 0$, $\Delta_{us} \neq 0$, $\Delta_{ds} = 0$;
5. CFL: $\Delta_{ud} \neq 0$, $\Delta_{ds} \neq 0$, $\Delta_{us} \neq 0$;

and their gapless versions. The resulting phase diagrams for intermediate and strong coupling are given in Figs. 5 and 6, resp. and constitute the main result of this work, which is summarized in the following statements:

1. Gapless phases occur only at high temperatures, above 50 MeV (intermediate coupling) or 60 MeV (strong coupling).
2. CFL phases occur only at rather high chemical potential, well above the chiral restoration transition, i.e. above 464 MeV (intermediate coupling) or 426 MeV (strong coupling).
3. Two-flavor quark matter for intermediate coupling is at low temperatures (T<20-30 MeV) in a mixed NQ-2SC phase, at high temperatures in the pure 2SC phase.
4. Two-flavor quark matter for strong coupling is in the 2SC phase with rather high critical temperatures of ~ 100 MeV.

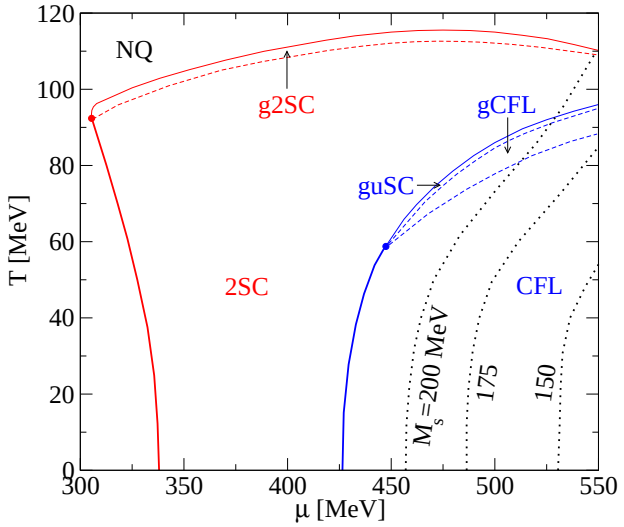

FIG. 6: Phase diagram of neutral three-flavor quark matter for strong diquark coupling $\eta = 1$. Line styles as in Fig. 3

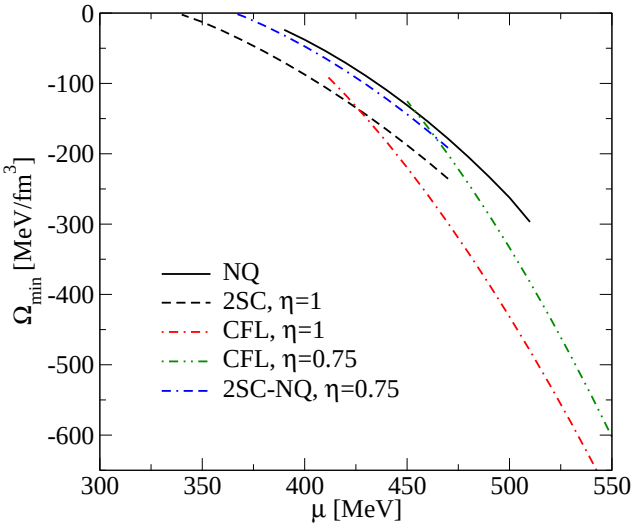

FIG. 7: Minima of the thermodynamical potential for neutral three-flavor quark matter at T=0 as a function of the quark chemical potential. Note that at a given coupling η the state with the lowest $\Omega_{\rm min}$ is attained and the physical pressure is $P = -\Omega_{\rm min}$.

5. The critical endpoint of first order chiral phase transitions is at (T,μ)=(44 MeV, 347 MeV) for intermediate coupling and at (92 MeV, 305 MeV) for strong coupling.

D. Quark matter equation of state

The various phases of quark matter presented in the previous section have been identified by minimizing the thermodynamic potential, Ω, in the order parameters, Δ_{ij} and ϕ_i. For a homogenous system, the pressure is $P = -\Omega_{min}$, see Fig. 7, where the μ-dependence of Ω_{min} is shown at $T = 0$ for the different competing phases. The lowest value of Ω_{min} corresponds to the negative value of the physical pressure. The intersection of two curves corresponds to a first order phase transition. All other thermodynamic quantities can be obtained from the thermodynamic potential by derivatives. At intermediate coupling, we have a first order transition from the NQ-2SC phase to the CFL phase, whereas at strong coupling the first order transition is from the 2SC phase to the CFL phase, with a lower critical energy density. In Fig. 8 the equation of state for cold three-flavor quark matter is given on a form suitable for the investigation of hydrodynamic stability of gravitating compact object, so-called quark stars. This is the topic for the next Subsection.

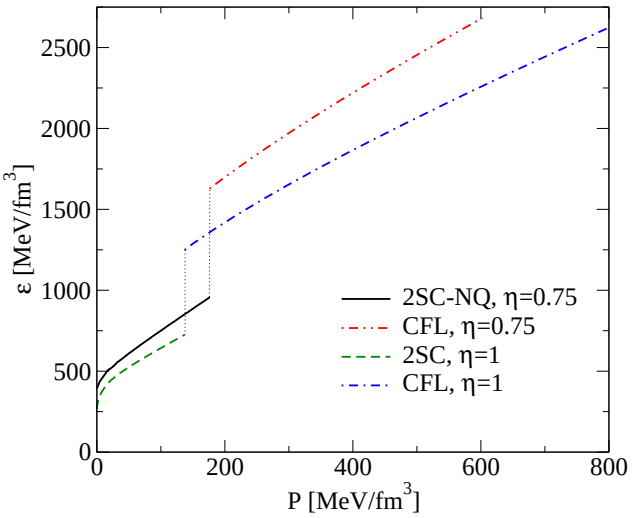

FIG. 8: Equation of state for three-flavor quark matter at T=0 with first order phase transitions. For intermediate diquark coupling ($\eta = 0.75$): from the mixed NQ-2SC phase to the CFL phase, for strong diquark coupling ($\eta = 1$): from the 2SC phase to the CFL phase.

E. Quark star configurations

The properties of spherically symmetric, static configurations of dense matter can be calculated with the well-known Tolman-Oppenheimer-Volkoff equations for hydrostatic equilibrium of self- gravitating matter, see also [46],

$$\frac{dP(r)}{dr} = -\frac{[\varepsilon(r) + P(r)][m(r) + 4\pi r^3 P(r)]}{r[r - 2m(r)]} \,. \qquad (23)$$

Here $\varepsilon(r)$ is the energy density and $P(r)$ the pressure at

distance r from the center of the star. The mass enclosed in a sphere with radius r is defined by

$$m(r) = 4\pi \int_0^r \varepsilon(r') r'^2 dr' \ . \qquad (24)$$

These equations are solved for given central baryon number densities, $n_B(r=0)$, thereby defining a sequence of quark star configurations. For the generalization to finite temperature configurations, see [47]. Hot quark stars have been discussed, e.g., in [48, 49, 50]. In Fig. 9 we show the stable configurations of quark stars for the three-flavor quark matter equation of state described above. The obtained mass radius relations allow for very compact selfbound objects, with a maximum radius that is less than 10 km. For intermediate diquark coupling, $\eta = 0.75$, stable stars consist of a NQ-2SC mixed phase with a maximum mass of 1.21 $M_\odot$. With incrasing density, a phase transition to the CFL phase renders the sequence unstable. For the strong diquark coupling, $\eta = 1$, quark matter is in the 2SC phase at low densities and the corresponding sequence of quark stars is stable up to a maximum mass of 1.33 $M_\odot$. The phase transition to CFL quark matter entails an instability that leads to a third family of stable stars, with masses in-between 1.30 and 1.33 $M_\odot$. For non-accreting compact stars the baryon number is an invariant during the cooling evolution. By comparing the masses of cold and hot isothermal configurations of quark stars of equal baryon number, the maximum mass defect (energy release due to cooling) can be calculated. The result for the strong diquark coupling, $\eta = 1$, is shown if Fig. 10. For an initial temperature of 40 MeV and a given baryon number of $N = 1.46\ N_\odot$, the initial mass is $M = 1.41\ M_\odot$. By cooling this object down to $T = 0$, a mass defect of $\Delta M = 0.1\ M_\odot$ occurs. For the chosen baryon number, $N = 1.46\ N_\odot$, there are two possible $T = 0$ configurations (twins). A hot star could thus evolve into the more compact mass-equivalent (twin) final state, if a fluctuation triggers the transition to a CFL phase in the core of the star. The structures of these two twin configurations are given in Fig. 11. The energy release of 0.1 $M_\odot$ is of the same order of magnitude as the energy release in supernova explosions and gamma-ray bursts. Disregarding the possible influence of a hadronic shell and the details regarding the heat transport, the cooling induced first order phase transition to the CFL phase could serve as a candidate process for the puzzling engine of these energetic phenomena [45, 50].

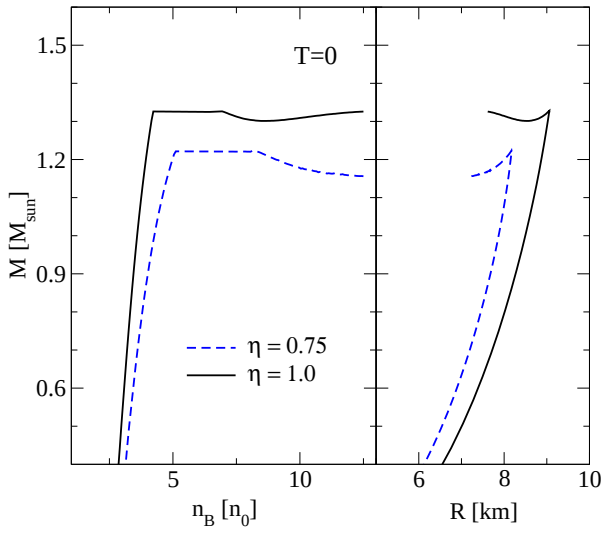

FIG. 9: Sequences of cold quark stars for the three-flavor quark matter equation of state described in the text. The rising branches in the mass-central density relation (left panel) indicate stable compact object configurations. The mass-radius relations (right panel) show that the three-flavor quark matter described in this paper leads to very compact self-bound objects. For intermediate diquark coupling, $\eta = 0.75$, stable stars consist of a mixed phase of NQ-2SC matter with a maximum mass of 1.21 $M_\odot$ (dashed line). At higher densities a phase transition to CFL quark matter occurs which entails a collapse of the star. For strong coupling, $\eta = 1$, the low density quark matter is in the 2SC phase and corresponding quark stars are stable up to a maximum mass of 1.326 $M_\odot$ (solid line). The phase transition to CFL quark matter entails an instability which at T=0 leads to a third family of stable stars for central densities above 9 n_0 and a mass twin window of 1.301 - 1.326 $M_\odot$.

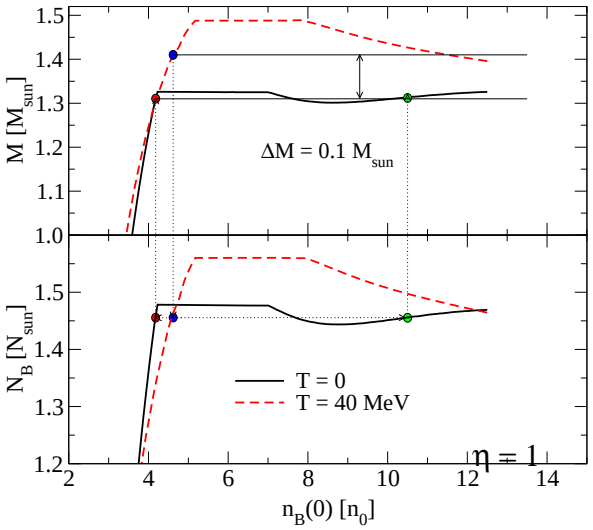

FIG. 10: Cooling an isothermal quark star configuration with initial mass $M = 1.41\ M_\odot$ at temperature $T = 40$ MeV under conservation of the given baryon number $N = 1.46\ N_\odot$ down to $T = 0$ leads to a mass defect $\Delta M = 0.1\ M_\odot$ for the strong coupling case ($\eta = 1.0$). Due to the twin structure at $T = 0$, two alternatives for the final state can be attained, a homogeneous 2SC quark star or a dense 2SC-CFL quark hybrid star.

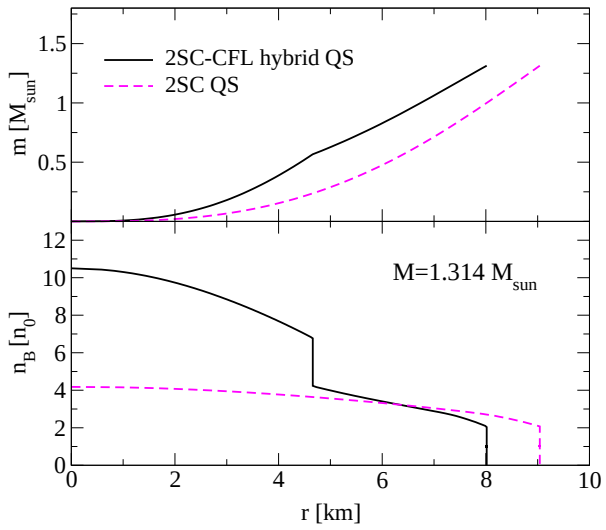

FIG. 11: Structure of two quark star (QS) configurations with $M = 1.314\ M_\odot$ (mass twins) for the three-flavor quark matter equation of state described in the text in the case of strong coupling ($\eta = 1$). The low-density twin has a radius of 9 km and is a homogeneous 2SC quark star, the high-density twin is more compact with a radius of 8 km and consists of a CFL quark matter core with 4.65 km radius and a 2SC quark matter shell.

IV. CONCLUSIONS

We have investigated the phase diagram of three-flavor quark matter within an NJL model under compact star constraints. Local color and electric charge neutrality is imposed for $\beta-$equilibrated superconducting quark matter. The constituent quark masses are selfconsistently determined. The model refrains from adopting the 't Hooft determinant interaction in the mean field Lagrangian as a realization of the $U_A(1)$ symmetry breaking. Instead, it is assumed that the $\eta - \eta'$ mass difference originates from an anomalous coupling of the pseudoscalar isosinglet fluctuation to the nonperturbative gluon sector, which gives no contribution to the quark thermodynamics at the mean field level. The resulting parametrization of this $SU_f(3)$ NJL model results in a stronger coupling than NJL models with a 't Hooft term and thus in different phase diagrams, cf. Ref. [41]. The diquark condensates are determined selfconsistently by minimization of the grand canonical thermodynamic potential. The various condensates are order parameters that characterize the different phases in the plane of temperature and quark chemical potential. These phases are in particular the NQ-2SC mixed phase, the 2SC, uSC, and CFL phases, as well as the corresponding gapless phases. We have investigated strong and intermediate diquark coupling strengths. It is shown that in both cases gapless superconducting phases does not occur at temperatures relevant for compact star evolution, i.e., below ~ 50 MeV. Three-flavor quark matter phases, e.g., the CFL phase, occur only at rather large chemical potential, so the existence of such phases in stable compact stars is questionable. The stability and stucture of isothermal quark star configurations are evaluated. For the strong diquark coupling, 2SC stars are stable up to a maximum mass of $1.33\ M_\odot$. A second family of more compact stars (twins) with a CFL quark matter core and masses in-between 1.30 and $1.33\ M_\odot$ are found to be stable. For intermediate coupling, the quark stars are composed of a mixed NQ-2SC phase up to a maximum mass of $1.21\ M_\odot$, where a phase transition to the CFL phase occurs and the configurations become unstable. When isothermal star configurations with an initial temperature of 40 MeV cools under conservation of baryon number, the mass defect is $0.1\ M_\odot$ for the strong diquark coupling. It is important to investigate the robustness of these statements, in particular by inlcuding nonlocal formfactors and by going beyond the mean-field level by including the effects of a hadronic medium on the quark condensates. Finally, any statement concerning the occurence and stability of quark matter in compact stars shall include an investigation of the influence of a hadronic shell [52, 53, 54] on the solutions of the equations of compact star structure.

V. ACKNOWLEDGEMENTS

F.S. acknowledges support from the Swedish National Graduate School of Space Technology. A.M.Ö. received support from Hacettepe University Research Fund, grant No. 02 02 602 001. D.B. thanks for partial support of the Department of Energy during the program INT-04-1 on *QCD and Dense Matter: From Lattices to Stars* at the University of Washington, where this work has been started. This work has been supported in part by the Virtual Institute of the Helmholtz Association under grant No. VH-VI-041. We are grateful to our colleagues in Darmstadt and Frankfurt who made the results of their study in Ref. [41] available to us prior to submission.

APPENDIX A: DISPERSION RELATIONS

The dispersion relations of the quasiparticles that appear in the expression for the thermodynamic potential (15) is the eigenvalues of the Nambu-Gorkov matrix (13). For each color and flavor combination of the eight component Nambu-Gorkov spinors, there is a corresponding 8x8 entry in this matrix; for three flavors and three colors (13) is a 72x72 matrix. The explicit form of this matrix can be represented by a table, where the rows and columns denote the flavor and color degrees of freedom

	q_{ur}	q_{ug}	q_{ub}	q_{dr}	q_{dg}	q_{db}	q_{sr}	q_{sg}	q_{sb}	$q^\dagger_{ur}$	$q^\dagger_{ug}$	$q^\dagger_{ub}$	$q^\dagger_{dr}$	$q^\dagger_{dg}$	$q^\dagger_{db}$	$q^\dagger_{sr}$	$q^\dagger_{sg}$	$q^\dagger_{sb}$
$q^\dagger_{ur}$	A_{ur}	0	0	0	0	0	0	0	0	0	0	0	0	D_{ud}	0	0	0	D_{us}
$q^\dagger_{ug}$	0	A_{ug}	0	0	0	0	0	0	0	0	0	0	$-D_{ud}$	0	0	0	0	0
$q^\dagger_{ub}$	0	0	A_{ub}	0	0	0	0	0	0	0	0	0	0	0	0	$-D_{us}$	0	0
$q^\dagger_{dr}$	0	0	0	A_{dr}	0	0	0	0	0	0	$-D_{ud}$	0	0	0	0	0	0	0
$q^\dagger_{dg}$	0	0	0	0	A_{dg}	0	0	0	0	D_{ud}	0	0	0	0	0	0	0	D_{ds}
$q^\dagger_{db}$	0	0	0	0	0	A_{db}	0	0	0	0	0	0	0	0	0	0	$-D_{ds}$	0
$q^\dagger_{sr}$	0	0	0	0	0	0	A_{sr}	0	0	0	0	$-D_{us}$	0	0	0	0	0	0
$q^\dagger_{sg}$	0	0	0	0	0	0	0	A_{sg}	0	0	0	0	0	0	$-D_{ds}$	0	0	0
$q^\dagger_{sb}$	0	0	0	0	0	0	0	0	A_{sb}	D_{us}	0	0	0	D_{ds}	0	0	0	0
q_{ur}	0	0	0	0	$D^\dagger_{ud}$	0	0	0	$D^\dagger_{us}$	B_{ur}	0	0	0	0	0	0	0	0
q_{ug}	0	0	0	$-D^\dagger_{ud}$	0	0	0	0	0	0	B_{ug}	0	0	0	0	0	0	0
q_{ub}	0	0	0	0	0	0	$-D^\dagger_{us}$	0	0	0	0	B_{ub}	0	0	0	0	0	0
q_{dr}	0	$-D^\dagger_{ud}$	0	0	0	0	0	0	0	0	0	0	B_{dr}	0	0	0	0	0
q_{dg}	$D^\dagger_{ud}$	0	0	0	0	0	0	0	$D^\dagger_{ds}$	0	0	0	0	B_{dg}	0	0	0	0
q_{db}	0	0	0	0	0	0	0	$-D^\dagger_{ds}$	0	0	0	0	0	0	B_{db}	0	0	0
q_{sr}	0	0	$-D^\dagger_{us}$	0	0	0	0	0	0	0	0	0	0	0	0	B_{sr}	0	0
q_{sg}	0	0	0	0	0	$-D^\dagger_{ds}$	0	0	0	0	0	0	0	0	0	0	B_{sg}	0
q_{sb}	$D^\dagger_{us}$	0	0	0	$D^\dagger_{ds}$	0	0	0	0	0	0	0	0	0	0	0	0	B_{sb}

. (A1)

Each entry is a 4x4 Hermitean matrix in Dirac space. The diagonal submatrices are

$$A_{i,\alpha} = \begin{bmatrix} p+\mu_{i,\alpha} & 0 & -M_i & 0 \\ 0 & -p+\mu_{i,\alpha} & 0 & -M_i \\ -M_i & 0 & -p+\mu_{i,\alpha} & 0 \\ 0 & -M_i & 0 & p+\mu_{i,\alpha} \end{bmatrix}, \quad \text{(A2)}$$

$$B_{j,\beta} = \begin{bmatrix} -p-\mu_{j,\beta} & 0 & M_j & 0 \\ 0 & p-\mu_{j,\beta} & 0 & M_j \\ M_j & 0 & p-\mu_{j,\beta} & 0 \\ 0 & M_j & 0 & -p-\mu_{j,\beta} \end{bmatrix}, \quad \text{(A3)}$$

whereas the off-diagonal blocks are given by

$$D_{i,j} = \begin{bmatrix} 0 & 0 & 0 & i\Delta_{i,j} \\ 0 & 0 & -i\Delta_{i,j} & 0 \\ 0 & i\Delta_{i,j} & 0 & 0 \\ -i\Delta_{i,j} & 0 & 0 & 0 \end{bmatrix}. \quad \text{(A4)}$$

The eigenvalues of (A1) are the quasiparticle energies, λ_a, that enter the thermodynamic potential (15), *i.e.*, the 72 dispersion relations of the various quark-quark and antiquark-antiquark excitations. These eigenvalues can be calculated using a standard numerical library. However, in order to reduce the computational cost, the matrix can be decomposed into a block-diagonal matrix by elementary row and column operations.

	q_{ur}	q_{dg}	q_{sb}	$q^\dagger_{ur}$	$q^\dagger_{dg}$	$q^\dagger_{sb}$	q_{ug}	$q^\dagger_{dr}$	q_{dr}	$q^\dagger_{ug}$	q_{ub}	$q^\dagger_{sr}$	q_{sr}	$q^\dagger_{ub}$	q_{db}	$q^\dagger_{sg}$	q_{sg}	$q^\dagger_{db}$
$q^\dagger_{ur}$	A_{ur}	0	0	0	D_{ud}	D_{us}	0	0	0	0	0	0	0	0	0	0	0	0
$q^\dagger_{dg}$	0	A_{dg}	0	D_{ud}	0	D_{ds}	0	0	0	0	0	0	0	0	0	0	0	0
$q^\dagger_{sb}$	0	0	A_{sb}	D_{us}	D_{ds}	0	0	0	0	0	0	0	0	0	0	0	0	0
q_{ur}	0	$D^\dagger_{ud}$	$D^\dagger_{us}$	B_{ur}	0	0	0	0	0	0	0	0	0	0	0	0	0	0
q_{dg}	$D^\dagger_{ud}$	0	$D^\dagger_{ds}$	0	B_{dg}	0	0	0	0	0	0	0	0	0	0	0	0	0
q_{sb}	$D^\dagger_{us}$	$D^\dagger_{ds}$	0	0	0	B_{sb}	0	0	0	0	0	0	0	0	0	0	0	0
$q^\dagger_{ug}$	0	0	0	0	0	0	A_{ug}	$-D_{ud}$	0	0	0	0	0	0	0	0	0	0
q_{dr}	0	0	0	0	0	0	$-D^\dagger_{ud}$	B_{dr}	0	0	0	0	0	0	0	0	0	0
$q^\dagger_{dr}$	0	0	0	0	0	0	0	0	A_{dr}	$-D_{ud}$	0	0	0	0	0	0	0	0
q_{ug}	0	0	0	0	0	0	0	0	$-D^\dagger_{ud}$	B_{ug}	0	0	0	0	0	0	0	0
$q^\dagger_{ub}$	0	0	0	0	0	0	0	0	0	0	A_{ub}	$-D_{us}$	0	0	0	0	0	0
q_{sr}	0	0	0	0	0	0	0	0	0	0	$-D^\dagger_{us}$	B_{sr}	0	0	0	0	0	0
$q^\dagger_{sr}$	0	0	0	0	0	0	0	0	0	0	0	0	A_{sr}	$-D_{us}$	0	0	0	0
q_{ub}	0	0	0	0	0	0	0	0	0	0	0	0	$-D^\dagger_{us}$	B_{ub}	0	0	0	0
$q^\dagger_{db}$	0	0	0	0	0	0	0	0	0	0	0	0	0	0	A_{db}	$-D_{ds}$	0	0
q_{sg}	0	0	0	0	0	0	0	0	0	0	0	0	0	0	$-D^\dagger_{ds}$	B_{sg}	0	0
$q^\dagger_{sg}$	0	0	0	0	0	0	0	0	0	0	0	0	0	0	0	0	A_{sg}	$-D_{ds}$
q_{db}	0	0	0	0	0	0	0	0	0	0	0	0	0	0	0	0	$-D^\dagger_{ds}$	B_{db}

(A5)

This matrix has one 24x24 and six 8x8 independent submatrices. Expressing these submatrices explicitely, using (A2-A4), the 24x24 matrix can be decomposed into two independent 12x12 submatrices by elementary row and column operations. Similarly, the six 8x8 matrices can be transformed into twelve independent 4x4 submatrices. There is a two-fold degeneracy due to the Nambu-Gorkov basis, each matrix appears both as $\mathcal{M}$ and $\mathcal{M}^\dagger$, so there are only one independent 12x12 matrix and six 4x4 matrices. The 12x12 matrix is

$$\mathcal{M}_{12} = \begin{bmatrix}
p+\mu_{ur} & 0 & 0 & -M_u & 0 & 0 & 0 & i\Delta_{ud} & i\Delta_{us} & 0 & 0 & 0 \\
0 & p+\mu_{dg} & 0 & 0 & -M_d & 0 & i\Delta_{ud} & 0 & i\Delta_{ds} & 0 & 0 & 0 \\
0 & 0 & p+\mu_{sb} & 0 & 0 & -M_s & i\Delta_{us} & i\Delta_{ds} & 0 & 0 & 0 & 0 \\
-M_u & 0 & 0 & -p+\mu_{ur} & 0 & 0 & 0 & 0 & 0 & i\Delta_{ud} & i\Delta_{us} & \\
0 & -M_d & 0 & 0 & -p+\mu_{dg} & 0 & 0 & 0 & 0 & i\Delta_{ud} & 0 & i\Delta_{ds} \\
0 & 0 & -M_s & 0 & 0 & -p+\mu_{sb} & 0 & 0 & 0 & i\Delta_{us} & i\Delta_{ds} & 0 \\
0 & -i\Delta_{ud} & -i\Delta_{us} & 0 & 0 & 0 & -p-\mu_{ur} & 0 & 0 & M_u & 0 & 0 \\
-i\Delta_{ud} & 0 & -i\Delta_{ds} & 0 & 0 & 0 & 0 & -p-\mu_{dg} & 0 & 0 & M_d & 0 \\
-i\Delta_{us} & -i\Delta_{ds} & 0 & 0 & 0 & 0 & 0 & 0 & -p-\mu_{sb} & 0 & 0 & M_s \\
0 & 0 & 0 & 0 & -i\Delta_{ud} & -i\Delta_{us} & M_u & 0 & 0 & p-\mu_{ur} & 0 & 0 \\
0 & 0 & 0 & -i\Delta_{ud} & 0 & -i\Delta_{ds} & 0 & M_d & 0 & 0 & p-\mu_{dg} & 0 \\
0 & 0 & 0 & -i\Delta_{us} & -i\Delta_{ds} & 0 & 0 & 0 & M_s & 0 & 0 & p-\mu_{sb}
\end{bmatrix}, \tag{A6}$$

and the 4x4 matrices are

$$\mathcal{M}_4 = \begin{bmatrix}
p+\mu_{i,\alpha} & -i\Delta_{i,j} & -M_i & 0 \\
i\Delta_{i,j} & -p-\mu_{j,\beta} & 0 & M_j \\
-M_i & 0 & -p+\mu_{i,\alpha} & -i\Delta_{i,j} \\
0 & M_j & i\Delta_{i,j} & p-\mu_{j,\beta}
\end{bmatrix}, \tag{A7}$$

for spinor products $ug-dr$, $ub-sr$, $db-sg$, $dr-ug$, $sr-ub$, and $sg-db$, respectively.

Since these matrices are Hermitean, the eigenvalues appear in $\pm$ pairs. Thus, in general, there are nine independent dispersion relations for quark-quark excitations

and nine for antiquark-antiquark excitations. The eigenvalues of (A6) must be calculated numerically. The eigenvalues of (A7) can be obtained analytically by solving for the roots of the quartic characteristic polynomial,

$$\lambda^4 + a_3\lambda^3 + a_2\lambda^2 + a_1\lambda + a_0 = 0, \qquad \text{(A8)}$$

where

$$\begin{aligned}
a_0 &= P^4 + \left(M_i^2 + M_j^2 + 2\Delta_{i,j}^2 - \mu_{i,\alpha}^2 - \mu_{j,\beta}^2\right) P^2 \\
&+ \left(\mu_{i,\alpha}\mu_{j,\beta} + M_i M_j + \Delta_{i,j}^2 + \mu_{i,\alpha} M_j + \mu_{j,\beta} M_i\right) \\
&\quad \left(\mu_{i,\alpha}\mu_{j,\beta} + M_i M_j + \Delta_{i,j}^2 - \mu_{i,\alpha} M_j - \mu_{j,\beta} M_i\right), \\
a_1 &= 2\left(\mu_{i,\alpha} - \mu_{j,\beta}\right) P^2 + 2\Delta_{i,j}^2\left(\mu_{i,\alpha} - \mu_{j,\beta}\right) \\
&+ 2\left(\mu_{i,\alpha} M_j^2 - \mu_{j,\beta} M_i^2 + \mu_{i,\alpha}^2\mu_{j,\beta} - \mu_{j,\beta}^2\mu_{i,\alpha}\right), \\
a_2 &= \mu_{i,\alpha}^2 + \mu_{j,\beta}^2 - 2P^2 - M_i^2 - M_j^2 - 2\Delta_{i,j}^2 - 4\mu_{i,\alpha}\mu_{j,\beta}, \\
a_3 &= -2\left(\mu_{i,\alpha} - \mu_{j,\beta}\right).
\end{aligned}$$

In the limit when $M_i = M_j = M$, which is approximately valid for the $ug - dr$ and $dr - ug$ quasiparticles, the four solutions are

$$\lambda = \frac{\mu_{i,\alpha} - \mu_{j,\beta}}{2} \pm \sqrt{\left(\frac{\mu_{i,\alpha} + \mu_{j,\beta}}{2} \pm E\right)^2 + \Delta_{i,j}^2}, \qquad \text{(A9)}$$

where $E = \sqrt{p^2 + M^2}$. This result is in agreement with [41]. More generally, the solutions of the quartic equation can be found in textbooks, see, e.g., [51]. In this work the eigenvalues of the 4x4 matrices were calculated with the exact solutions of the quartic equation and the eigenvalues of the 12x12 matrix were calculated with LAPACK. The momentum integral in (15) was calculated with a Gaussian quadrature. The minimization of the thermodynamic potential was performed with conjugate gradient methods, choosing the initial values of the variational parameters carefully, and then comparing the free energies of the various minima. The color and electric charges were neutralized with a globally convergent Newton-Raphson method in multidimensions.

Gapless excitations/dispersion relations are characterized by a non-zero condensate, $\Delta_{i,j}$, and a corresponding dispersion relation that is zero for at least one value of the quasiparticle momentum, *i.e.*, the dispersion relation reaches the Fermi surface and there is no forbidden energy band.

[1] R. Rapp *et al.*, Phys. Rev. Lett. **81** (1998) 53.
[2] M. Alford, K. Rajagopal and F. Wilczek, Phys. Lett. **B450** (1999) 325.
[3] D. Blaschke and C. D. Roberts, Nucl. Phys. A **642** (1998) 197.
[4] B.C. Barrois, Nucl. Phys. **B129** (1977) 390.
[5] D. Bailin and A. Love, Phys. Rep. **107** (1984) 325.
[6] K. Rajagopal and F. Wilczek, arXiv:hep-ph/0011333.
[7] M. G. Alford, Ann. Rev. Nucl. Part. Sci. **51** (2001) 131.
[8] M. Buballa, Phys. Rep. **407** (2005) 205.
[9] A. Schmitt, Phys. Rev. D **71**, 054016 (2005)
[10] D. Blaschke, N.K. Glendenning, A. Sedrakian (Eds.), *Physics of Neutron Star Interiors* (Springer, Heidelberg, 2001).
[11] D.K. Hong et al. (Eds.), *Compact Stars: The quest for new states of matter* (World Scientific, Singapore, 2004).
[12] D. Blaschke, D. Sedrakian (Eds.), *Superdense QCD Matter in Compact Stars* (Springer, Heidelberg, 2005).
[13] J. E. Horvath, O. G. Benvenuto and H. Vucetich, Phys. Rev. D **44**, 3797 (1991).
[14] D. Blaschke, T. Klähn and D. N. Voskresensky, Astrophys. J. **533** (2000) 406.
[15] D. Page, M. Prakash, J. M. Lattimer and A. Steiner, Phys. Rev. Lett. **85** (2000) 2048.
[16] D. Blaschke, H. Grigorian and D. N. Voskresensky, Astron. Astrophys. **368** (2001) 561.
[17] H. Grigorian, D. Blaschke and D. Voskresensky, Phys. Rev. **C** (2005) in press; [arXiv:astro-ph/0411619].
[18] D. Blaschke, D. M. Sedrakian and K. M. Shahabasian, Astron. Astrophys. **350** (1999) L47.
[19] M. G. Alford, J. Berges and K. Rajagopal, Nucl. Phys. B **571** (2000) 269.
[20] K. Iida and G. Baym, Phys. Rev. D **66** (2002) 014015.
[21] D. M. Sedrakian, D. Blaschke, K. M. Shahabasian and D. N. Voskresensky, Phys. Part. Nucl. **33** (2002) S100.
[22] D. K. Hong, S. D. H. Hsu and F. Sannino, Phys. Lett. B **516** (2001) 362.
[23] R. Ouyed and F. Sannino, Astron. Astrophys. **387** (2002) 725.
[24] D. N. Aguilera, D. Blaschke and H. Grigorian, Astron. Astrophys. **416** (2004) 991.
[25] R. Ouyed, R. Rapp and C. Vogt, arXiv:astro-ph/0503357.
[26] F. Neumann, M. Buballa and M. Oertel, Nucl. Phys. A **714** (2003) 481.
[27] M. Oertel and M. Buballa, arXiv:hep-ph/0202098.
[28] C. Gocke, D. Blaschke, A. Khalatyan and H. Grigorian, arXiv:hep-ph/0104183.
[29] M. Alford and K. Rajagopal, JHEP **0206** (2002) 031.
[30] A. W. Steiner, S. Reddy and M. Prakash, Phys. Rev. D **66** (2002) 094007.
[31] M. G. Alford, C. Kouvaris and K. Rajagopal, Phys. Rev. Lett. **92** (2004) 222001.
[32] M. Alford, C. Kouvaris and K. Rajagopal, Phys. Rev. D **71**, 054009 (2005).
[33] S. B. Ruster, I. A. Shovkovy and D. H. Rischke, Nucl. Phys. A **743**, 127 (2004).
[34] I. Shovkovy and M. Huang, Phys. Lett. B **564** (2003) 205.
[35] M. Huang & I. Shovkovy, Nucl. Phys. **A729** (2003) 835.
[36] M. G. Alford, K. Rajagopal and F. Wilczek, Nucl. Phys. **B537**, 443 (1999).
[37] D. Blaschke, H. P. Pavel, V. N. Pervushin, G. Ropke and M. K. Volkov, Phys. Lett. B **397** (1997) 129.
[38] L. von Smekal, A. Mecke and R. Alkofer, arXiv:hep-ph/9707210.

[39] H. B. Nielsen, M. Rho, A. Wirzba and I. Zahed, Phys. Lett. B **281** (1992) 345.
[40] R. Alkofer, P. A. Amundsen and H. Reinhardt, Phys. Lett. B **218** (1989) 75.
[41] S. B. Ruster, V. Werth, M. Buballa, I. A. Shovkovy and D. H. Rischke, arXiv:hep-ph/0503184.
[42] L. P. Gor'kov, Zh. Eksp. Teor. Fiz. **36** (1959) 1918.
[43] Y. Nambu, Phys. Rev. **117** (1960) 648.
[44] J. I. Kapusta, *Finite-temperature field theory* (University Press, Cambridge, 1989).
[45] D. N. Aguilera, D. Blaschke and H. Grigorian, arXiv:hep-ph/0412266.
[46] N. K. Glendenning, *Compact Stars* (Springer, New York, 2000)
[47] S. L. Shapiro and S. A. Teukolsky, *Black Holes, White Dwarfs, And Neutron Stars* (Wiley, New York, 1983).
[48] C. Kettner, F. Weber, M. K. Weigel and N. K. Glendenning, Phys. Rev. D **51** (1995) 1440.
[49] D. Blaschke, H. Grigorian, G. S. Poghosyan, C. D. Roberts and S. M. Schmidt, Phys. Lett. B **450** (1999) 207.
[50] D. Blaschke, S. Fredriksson, H. Grigorian and A. M. Oztas, Nucl. Phys. A **736** (2004) 203.
[51] M. Abramowitz & I. A. Stegun, *Handbook of Mathematical Functions with Formulas, Graphs, and Mathematical Tables* (Dover, New York, 1972), pp. 17-18.
[52] M. Baldo, M. Buballa, F. Burgio, F. Neumann, M. Oertel and H. J. Schulze, Phys. Lett. B **562** (2003) 153.
[53] I. Shovkovy, M. Hanauske and M. Huang, Phys. Rev. D **67** (2003) 103004.
[54] H. Grigorian, D. Blaschke and D. N. Aguilera, Phys. Rev. C **69** (2004) 065802.